Identification of an Elaborate Complex Mediating Postsynaptic Inhibition

Akiyoshi Uezu[1], **Daniel J. Kanak**[1,*], **Tyler W.A. Bradshaw**[1,*], **Erik J. Soderblom**[1,2], **Christina M. Catavero**[1], **Alain C. Burette**[3], **Richard J. Weinberg**[3], and **Scott H. Soderling**[1,4,†]

[1]The Department of Cell Biology, Duke University Medical School, Durham, North Carolina, USA

[2]Duke Proteomics and Metabolomics Shared Resource and Duke Center for Genomic and Computational Biology, Duke University Medical School, Durham, North Carolina, USA

[3]Department of Cell Biology and Physiology, University of North Carolina, Chapel Hill, North Carolina, USA. Neuroscience Center, University of North Carolina, Chapel Hill, North Carolina, USA

[4]The Department of Neurobiology, Duke University Medical School, Durham, North Carolina, USA

Abstract

Inhibitory synapses dampen neuronal activity through postsynaptic hyperpolarization. The composition of the inhibitory postsynapse and the mechanistic basis of its regulation, however, remains poorly understood. We used an *in vivo* chemico-genetic proximity-labeling approach to discover inhibitory postsynaptic proteins. Quantitative mass spectrometry not only recapitulated known inhibitory postsynaptic proteins, but also revealed a large network of new proteins, many of which are either implicated in neurodevelopmental disorders or are of unknown function. CRISPR-depletion of one of these previously uncharacterized proteins, InSyn1, led to decreased postsynaptic inhibitory sites, reduced frequency of miniature inhibitory currents, and increased excitability in the hippocampus. Our findings uncover a rich and functionally diverse assemblage of previously unknown proteins that regulate postsynaptic inhibition and might contribute to developmental brain disorders.

Introduction

Two anatomically distinct classes of synapses are present in the central nervous system: excitatory synapses, predominantly localized to postsynaptic spines; and inhibitory synapses, in which the postsynapse is typically embedded in the soma and dendritic shaft(1). Purification and analysis of the protein complexes of the excitatory postsynapse have led to

fundamental insights in neurobiology. These insights include how receptor trafficking, synaptic adhesion, cytoskeletal remodeling, and protein phosphorylation contribute to the synaptic plasticity underlying learning and memory(2, 3). Moreover, genetic perturbations of excitatory postsynaptic proteins are strongly implicated in developmental brain disorders and psychiatric conditions(4, 5).

In contrast, the biochemical purification and analysis of the inhibitory postsynaptic density (iPSD) has remained largely intractable. Accordingly, the molecular basis of postsynaptic inhibitory synapse regulation and its contribution to neurodevelopmental disorders is poorly understood. Recently, an affinity purification approach, BioID, has been developed that utilizes a promiscuous *E.coli* biotinylation enzyme BirA^{R118G} (here termed BirA) fused to a bait protein expressed in cells(6). BirA-dependent covalent biotinylation occurs within 10–50 nm of the bait protein and allows for efficient isolation and analysis of proximal proteins by streptavidin-based affinity purification and mass spectrometry(7). Compared to affinity purification methods, the BioID reaction is executed *in situ*, thus enabling the capture of protein complexes, including transient interactions and insoluble proteins from subcellular compartments refractory to biochemical isolation(8).

We adapted the BioID approach to enable *in vivo* BioID (iBioID) of synaptic complexes in mouse brain. We virally expressed inhibitory or excitatory PSD proteins fused to BirA to capture and purify their associated proteins. The method labels the corresponding postsynaptic structures *in vivo,* and enabled the identification of virtually all of the known proteins of the iPSD. It also revealed a large number of previously unknown proteins, including a rich diversity of transmembrane and signaling proteins. These results provide a molecular prospectus for the deeper understanding of synaptic physiology that was until now largely confined to the excitatory PSD.

In Vivo Capture of Synaptic Protein Complexes

Gephyrin is the major scaffolding protein organizing the iPSD structure, interacting directly with GlyRs or GABA$_A$Rs and other molecules such as neuroligin-2 (NL2) and collybistin (Arhgef9)(9–11). To label proteins associated with synaptic proteins in the context of native tissue *in vivo*, we created Adeno-associated viral (AAV) constructs for the expression of gephyrin- and PSD-95-fused BirA, targeting the proteomes of inhibitory and excitatory postsynapses, respectively (Fig. 1A). To control for synapse specificity of biotinylation we also expressed soluble BirA, which non-specifically biotinylates proteins throughout the neuron. Each construct was validated by immunocytochemistry to determine its localization and synaptic site of biotinylation (Fig. 1B). To label synaptic structures *in vivo* we developed a protocol that maximizes the number of synapses labeled by injection of AAV into the cortex of postnatal day 0 (P0) mouse pups, followed by seven days of daily doses of exogenous biotin (Fig. 1C). Immunohistochemical analysis validates the approach for *in vivo* biotinylation (Fig. 1D), yielding punctate labeling of synaptic sites in brain tissue (Fig. 1E). Immuno-electron microscopy verified that biotinylation occurred at symmetric (i.e. inhibitory) synapses for BirA-gephyrin, and at asymmetric (i.e. excitatory) postsynaptic sites for PSD-95-BirA (Fig. 1F, G). Subcellular sites of background staining (perhaps due to overexpression or detection of endogenous biotinylated carboxylases) were also noted to

guide the final proteomic analysis (Fig. S1A and Table S1). Purification of biotinylated proteins from neurons expressing each BirA fusion protein and subsequent immunoblotting for known components of inhibitory (collybistin) and excitatory (NR2B and GluA1) synapses verified that each bait specifically labeled components of these synaptic sites, versus the non-specific labeling of our negative control, soluble BirA (Fig. 1H).

Discovery of the Inhibitory Postsynaptic Proteome

To pilot the identification of proteins labeled by iBioID, four cohorts were prepared each for BirA, PSD-95-BirA, and BirA-gephyrin using the labeling protocol outlined in Fig. 1C. Biotinylated proteins purified by streptavidin affinity purification were identified by liquid chromatography tandem mass spectrometry (LC/MS/MS). In total, 928 unique proteins were identified from twelve separate LC/MS/MS runs, with unique compliments of proteins enriched over BirA in each synaptic fraction (Fig. S1B–E, Table S2). Analysis of the gephyrin-BirA fraction confirmed several proteins reported to reside at the iPSD(10, 12), including Arhgef9/collybistin, VASP family proteins Mena and Evl, and IQSEC3, and two proteins of unknown function, which we termed "inhibitory synaptic proteins 1 and 2" or InSyn1 (UPF0583 protein C15orf59 homolog) and InSyn2 (Protein Fam196a). This pilot study suggested that while the BirA-gephyrin is highly specific, increased coverage of the iPSD would be desirable. We therefore expanded the analysis of the iPSD by performing the MS/MS analysis using more sensitive instrumentation, and by including additional BirA-fusion proteins to further label the iPSD (collybistin-BirA and InSyn1-BirA) (Fig. S1, F and G). InSyn1 was included since functional studies (described below) verified it was an important component of the iPSD. Quantitative high-resolution LC/MS/MS was then performed for each sample (PSD dataset: BirA versus PSD-95; iPSD dataset: BirA versus gephyrin, collybistin, InSyn1) in biological triplicates (7–8 mice per biological fraction). For the excitatory PSD-95 dataset 18,207 peptides corresponding to 2,533 unique proteins were quantified, whereas 17,024 peptides corresponding to 2,183 proteins were quantified from the iPSD datasets. Proteins were considered significantly enriched in the bait fraction if their average BirA-fusion protein levels were at least 2-fold greater than the BirA-alone fractions with p-values <0.05. Based on these criteria, 121 ePSD proteins (Fig. S2) were specifically labeled by PSD-95-BirA (Table S3). More than 95% of the ePSD proteins identified by iBioID were previously known ePSD components as identified by traditional PSD biochemical fractionation and mass spectrometry (116 of 121 proteins), demonstrating the specificity of the method. These proteins included glutamate receptors, scaffolding proteins, and signaling proteins of excitatory synaptic complexes. The iPSD dataset identified a combined 181 proteins (Table S4), including nearly all previously reported proteins of the iPSD (13), suggesting that coverage of the iPSD had approached saturation (Fig. 2). We also identified a large number of proteins not previously known to reside at the iPSD, including trafficking proteins, cytoskeletal regulatory proteins, integral membrane proteins, and several protein kinases and phosphatases (Fig. 2B). Many of these proteins (27/181) are encoded by genes implicated in either seizure susceptibility in humans or mice, or other brain disorders such as intellectual disability (ID) (Table S4). Comparison of iPSD and PSD95 identified 17 proteins shared by the two datasets, 50% of which are signaling proteins (Table S5).

Candidate iPSD proteins co-localize and co-immunoprecipitate with gephyrin

To validate our iBioID results, select iPSD proteins (InSyn1, InSyn2, IQSEC3, Collybistin [Arhgeg9], and PX-RICS [Arhgap32]) were cloned and co-expressed in primary neuronal cells with GPHN.FingR-GFP, a marker of endogenous gephyrin(14) (Fig. 3A). Collybistin served as a positive control, while PSD-95 co-localization served as negative control. Quantification of co-localizing pixels (Fig. 3B) demonstrated that each iPSD protein significantly overlapped with endogenous gephyrin. Each candidate protein was also tested in co-immunoprecipitation experiments. Epitope-tagged iPSD proteins specifically co-precipitated with GFP-gephyrin, including InSyn1 and InSyn2 (Fig. 3C–F).

InSyn1 and InSyn2 are iPSD proteins functionally important for GABAergic inhibition

InSyn1 is a previously uncharacterized protein that lacks protein domains of known function, but whose extensive iBioID interactions with core components of the iPSD (gephyrin, neuroligin-2, collybistin, $GABA_AR$ subunit beta-3), suggested a central role in $GABA_AR$-dependent synaptic inhibition. To test if InSyn1 is functionally important for synaptic inhibition, we used single-cell CRISPR-mediated depletion of the endogenous protein (15) (Fig. 4A). $GABA_AR$-mediated miniature inhibitory postsynaptic currents (mIPSCs) were recorded from CA1 pyramidal cells in hippocampal slices that were biolistically transfected with GFP, spCas9, and validated InSyn1 gRNA (Fig. 4B). Untransfected (GFP-negative) cells located within a 400 μm radius from GFP-positive cells served as controls, and gRNA specificity was tested by re-expression of Cas9-resistant cDNAs (Fig. 4B). Inhibitory currents were confirmed to be GABAergic because they were reversibly abolished in the presence of bicuculline (1 μM, Fig. S3A). To verify the efficacy of the CRISPR strategy for functional testing of iPSD synaptic proteins, we targeted the obligatory γ2 subunit of the $GABA_AR$, finding a complete abolition of mIPSCs (Fig. S3B). We also verified that biolistic transfection of GFP alone did not alter mIPSC characteristics (Fig. S3,C–E). Using sgRNA targeting InSyn1 with and without an InSyn1 rescue construct, we found a significant and reversible 69% increase in mIPSC inter-event intervals (IEI); the difference in amplitude was not statistically significant (Fig. 4C–D). The effect of InSyn1 gRNA was specific to inhibitory currents, as AMPAR-mediated mEPSC characteristics were unaltered (Fig. 5E–F). To further test the predictive value of the iPSD dataset, we performed analogous experiments targeting InSyn2. Depletion of InSyn2 resulted in a specific and reversible 62% increase of mIPSC IEI (Fig. S4).

Given the large effect of InSyn1 depletion on mIPSC frequency, we next asked whether the inhibitory deficits evident at the single-cell level manifest at the network level. We used a carbachol-induced model of the "awake-state" gamma rhythm, which is critically dependent on GABAergic inhibition(16). P0 *Rosa26-LSL-Cas9*(17) pups were bilaterally infused with AAV:*Cre/InSyn1:gRNA* virus or AAV:*Cre/(-):gRNA* control virus in the cortex and hippocampus (Fig. 4G). In the majority of acute slices prepared from control mice, carbachol (CCH) induced a pure gamma rhythm with peak frequencies of ~30–40 Hz (Fig.

4H, *top trace*). In contrast, the majority of InSyn1 gRNA-infected slices exhibited a mixture of gamma oscillations with hyperexcitable events including interictal epileptiform discharges (IEDs, Fig. 4H, *middle trace*) and prolonged (2–5 s) bursts resembling ictal discharges (Fig. 4H, *lower trace*). Overall, we found a 4-fold increase in the proportion of slices with IEDs (Fig. 4I). Power spectral analysis revealed a 2.2-fold increase in low-frequency (0–15 Hz) power corresponding to epileptiform activity, and a 42% reduction in gamma-band (20–50 Hz) power (Fig. 4J). These effects likely reflect loss of GABAergic inhibition, as bath application of low concentrations of bicuculline (0.5 μM steps) abolished the gamma rhythm in control slices and induced epileptiform activity similar to that seen in InSyn1 gRNA slices (Fig. S3F).

InSyn1 functions via the dystrophin complex at inhibitory synaptic sites

We next analyzed how InSyn1 functions at inhibitory synapses by further examining its interacting proteins and how its loss alters the iPSD. InSyn1-GFP expressed in hippocampal neurons co-localized with gephyrin in dendritic shafts (Fig. S5A). InSyn1-GFP or GFP alone was expressed in the frontal cortex and hippocampus of C57BL/6 mice using AAV and precipitated using GFP-trap resin. InSyn1-GFP and GFP-alone co-precipitating proteins were analyzed by LC/MS/MS and compared. InSyn1 pulldown fractions were enriched with 86 proteins (Fig. 5A. Table S6), forming a highly interconnected protein-protein interaction network that included many proteins in the iBioID iPSD (including InSyn2, gephyrin, and Iqsec3) (Fig. 5B).

Among the most enriched proteins were seven components of the dystrophin complex, including dystrophin (DMD), dystrobrevin alpha and beta (Dtna and Dtnb), and alpha-1, beta-1, and beta-2-syntrophins (Snta1, Sntb1, Sntb2) (Fig. 5C). In brain, the dystrophin complex is a component of the iPSD, and its loss in muscular dystrophies contributes to cognitive impairments and epilepsy(18). InSyn1-BirA also captured multiple components of the dystrophin complex (Fig. 2A–B), suggesting it forms a physical complex with both gephyrin and the dystrophin complex. Affinity purified anti-InSyn1 antibody recognized a band of approximately 50–52 kDa from cells transfected with HA-InSyn1 or from mouse brain extract (Fig. S5B). Immunofluorescence demonstrated that InSyn1 co-localizes with endogenous alpha-dystroglycan (α-DG); this punctate staining was lost in neurons cultured from *Rosa26-LSL-Cas9* mice and infected with AAV:Cre/InSyn1:gRNA virus (Fig. 5D). Quantitative analysis demonstrated that InSyn1 gRNA-infected neurons had significant reductions in densities of both α-DG and GABA$_A$R puncta and a significant a reduction in their co-localization (Fig. 5E–H). In contrast, the density of PSD-95 puncta was unaffected (Fig. 5I). These results are consistent with the reduced mIPSC frequencies we observed in single neuron CRISPR-mediated InSyn1 depletion, supporting the notion that the loss of postsynaptic sites of inhibition occurs in its absence.

Discussion

We report here the *in vivo* application of the BioID approach to analyze the local proteome of the postsynaptic compartment of inhibitory synapses by quantitative mass spectrometry. Comparing this approach to prior reports of the iPSD using affinity purification(19–21),

iBioID offers important advantages. Nearly all proteins previously reported to exist at the iPSD were identified. iBioID also identified 140 proteins not previously associated with the iPSD, including a wide range of signaling, transmembrane, structural, and uncharacterized proteins. Although we included multiple controls (BirA alone, EM analysis of nonspecific label) for the overexpression strategy, we anticipate future studies with endogenous proteins fused to BirA will likely further refine the iBioID approach.

To validate our results and to determine how the iPSD is regulated, we focused on two proteins of unknown function, InSyn1 and InSyn2, that associate with several core components of the iPSD. When expressed in neurons, both co-localized with endogenous gephyrin and their loss resulted in a significant reduction in mIPSC frequency, confirming the validity of the iBioID approach. The mechanism of reduced mIPSC frequency for InSyn1 is likely through the disruption of the ability of InSyn1 to form complexes with both gephyrin and the dystrophin complex at the iPSD. Loss of dystrophin might also lead to a secondary trans-synaptic effect on presynaptic release probability through its ability to bind neurexins(22, 23).

Twenty-seven of the proteins of the iPSD, including several proteins first identified here, are implicated by either human or mouse genetics in seizure susceptibility/familial epilepsy, ID, or autism (Fig. 2G). Of the newly identified iPSD proteins implicated in developmental disorders, many are signaling proteins or are proteins of unknown functions (Supplemental Discussion). It is also interesting to note that 17 proteins overlapped between the inhibitory and excitatory PSD fractions. These could reflect dual synapses (spines containing gephyrin(24)) or might represent signaling proteins that transit between synapse types to facilitate synaptic crosstalk.

Our results indicate the composition of the iPSD is far more complex than previously appreciated. This concept is in line both with emerging evidence of inhibitory synaptic plasticity at the postsynaptic specialization(25–32), and with our molecular evidence that the iPSD is associated with a variety of signaling proteins, analogous to that of excitatory synapses. The identification of the iPSD proteome provides a rational basis for investigating fundamental mechanisms that regulate synaptic inhibition. It also establishes a new reference frame to ascertain how perturbations of this protein complex may contribute to developmental brain disorders.

Supplementary Material

Refer to Web version on PubMed Central for supplementary material.

Acknowledgments

References and Notes

1. Gray EG. Axo-somatic and axo-dendritic synapses of the cerebral cortex: an electron microscope study. Journal of anatomy. 1959; 93:420–433. [PubMed: 13829103]

2. Malenka RC, Bear MF. LTP and LTD: an embarrassment of riches. Neuron. 2004; 44:5–21. [PubMed: 15450156]

3. Kennedy MB, Beale HC, Carlisle HJ, Washburn LR. Integration of biochemical signalling in spines. Nat Rev Neurosci. 2005; 6:423–434. [PubMed: 15928715]

4. Grant SG. Synaptopathies: diseases of the synaptome. Curr Opin Neurobiol. 2012; 22:522–529. [PubMed: 22409856]

5. Volk L, Chiu SL, Sharma K, Huganir RL. Glutamate synapses in human cognitive disorders. Annu Rev Neurosci. 2015; 38:127–149. [PubMed: 25897873]

6. Roux KJ, Kim DI, Raida M, Burke B. A promiscuous biotin ligase fusion protein identifies proximal and interacting proteins in mammalian cells. The Journal of cell biology. 2012; 196:801–810. [PubMed: 22412018]

7. Kim DI, et al. Probing nuclear pore complex architecture with proximity-dependent biotinylation. Proc Natl Acad Sci U S A. 2014; 111:E2453–2461. [PubMed: 24927568]

8. Yao Z, Petschnigg J, Ketteler R, Stagljar I. Application guide for omics approaches to cell signaling. Nat Chem Biol. 2015; 11:387–397. [PubMed: 25978996]

9. Poulopoulos A, et al. Neuroligin 2 drives postsynaptic assembly at perisomatic inhibitory synapses through gephyrin and collybistin. Neuron. 2009; 63:628–642. [PubMed: 19755106]

10. Tyagarajan SK, Fritschy JM. Gephyrin: a master regulator of neuronal function? Nat Rev Neurosci. 2014; 15:141–156. [PubMed: 24552784]

11. Prior P, et al. Primary structure and alternative splice variants of gephyrin, a putative glycine receptor-tubulin linker protein. Neuron. 1992; 8:1161–1170. [PubMed: 1319186]

12. Um JW, et al. IQ Motif and SEC7 Domain-containing Protein 3 (IQSEC3) Interacts with Gephyrin to Promote Inhibitory Synapse Formation. The Journal of biological chemistry. 2016; 291:10119–10130. [PubMed: 27002143]

13. Known iPSD proteins included eight $GABA_A$ receptor subunits, inhibitory transmembrane adhesion proteins (e.g. neuroligin-2(33–35), Slitrk3(36) and neuroplastin(37, 38)), as well as signaling- and actin-associated proteins such as Trim3(39), Enah(40), profilin(41), and dystrophin complex proteins (including alpha-1-syntrophin, dystrobrevin alpha, and dystrophin)(42).

14. Gross GG, et al. Recombinant probes for visualizing endogenous synaptic proteins in living neurons. Neuron. 2013; 78:971–985. [PubMed: 23791193]

15. Incontro S, Asensio CS, Edwards RH, Nicoll RA. Efficient, complete deletion of synaptic proteins using CRISPR. Neuron. 2014; 83:1051–1057. [PubMed: 25155957]

16. Mann EO, Suckling JM, Hajos N, Greenfield SA, Paulsen O. Perisomatic feedback inhibition underlies cholinergically induced fast network oscillations in the rat hippocampus in vitro. Neuron. 2005; 45:105–117. [PubMed: 15629706]

17. Platt RJ, et al. CRISPR-Cas9 knockin mice for genome editing and cancer modeling. Cell. 2014; 159:440–455. [PubMed: 25263330]

18. Pane M, et al. Duchenne muscular dystrophy and epilepsy. Neuromuscul Disord. 2013; 23:313–315. [PubMed: 23465656]

19. Heller EA, et al. The biochemical anatomy of cortical inhibitory synapses. PLoS One. 2012; 7:e39572. [PubMed: 22768092]

20. Kang Y, et al. A combined transgenic proteomic analysis and regulated trafficking of neuroligin-2. The Journal of biological chemistry. 2014; 289:29350–29364. [PubMed: 25190809]

21. Nakamura Y, et al. Proteomic characterization of inhibitory synapses using a novel pHluorin-tagged GABAAR alpha2 subunit knock-in mouse. The Journal of biological chemistry. 2016

22. Sugita S, et al. A stoichiometric complex of neurexins and dystroglycan in brain. The Journal of cell biology. 2001; 154:435–445. [PubMed: 11470830]

23. Michele DE, et al. Post-translational disruption of dystroglycan-ligand interactions in congenital muscular dystrophies. Nature. 2002; 418:417–422. [PubMed: 12140558]

24. Villa KL, et al. Inhibitory Synapses Are Repeatedly Assembled and Removed at Persistent Sites In Vivo. Neuron. 2016; 89:756–769. [PubMed: 26853302]

25. Bourne JN, Harris KM. Coordination of size and number of excitatory and inhibitory synapses results in a balanced structural plasticity along mature hippocampal CA1 dendrites during LTP. Hippocampus. 2011; 21:354–373. [PubMed: 20101601]

26. Lushnikova I, Skibo G, Muller D, Nikonenko I. Excitatory synaptic activity is associated with a rapid structural plasticity of inhibitory synapses on hippocampal CA1 pyramidal cells. Neuropharmacology. 2011; 60:757–764. [PubMed: 21187106]

27. Niwa F, et al. Gephyrin-independent GABA(A)R mobility and clustering during plasticity. PLoS One. 2012; 7:e36148. [PubMed: 22563445]

28. Dejanovic B, et al. Palmitoylation of gephyrin controls receptor clustering and plasticity of GABAergic synapses. PLoS biology. 2014; 12:e1001908. [PubMed: 25025157]

29. Petrini EM, et al. Synaptic recruitment of gephyrin regulates surface GABAA receptor dynamics for the expression of inhibitory LTP. Nat Commun. 2014; 5:3921. [PubMed: 24894704]

30. Flores CE, et al. Activity-dependent inhibitory synapse remodeling through gephyrin phosphorylation. Proc Natl Acad Sci U S A. 2015; 112:E65–72. [PubMed: 25535349]

31. Chen JL, et al. Clustered dynamics of inhibitory synapses and dendritic spines in the adult neocortex. Neuron. 2012; 74:361–373. [PubMed: 22542188]

32. van Versendaal D, et al. Elimination of inhibitory synapses is a major component of adult ocular dominance plasticity. Neuron. 2012; 74:374–383. [PubMed: 22542189]

33. Varoqueaux F, Jamain S, Brose N. Neuroligin 2 is exclusively localized to inhibitory synapses. Eur J Cell Biol. 2004; 83:449–456. [PubMed: 15540461]

34. Graf ER, Zhang X, Jin SX, Linhoff MW, Craig AM. Neurexins induce differentiation of GABA and glutamate postsynaptic specializations via neuroligins. Cell. 2004; 119:1013–1026. [PubMed: 15620359]

35. Chih B, Engelman H, Scheiffele P. Control of excitatory and inhibitory synapse formation by neuroligins. Science (New York, NY). 2005; 307:1324–1328.

36. Takahashi H, et al. Selective control of inhibitory synapse development by Slitrk3-PTPdelta trans-synaptic interaction. Nat Neurosci. 2012; 15:398, S381–382.

37. Beesley PW, Herrera-Molina R, Smalla KH, Seidenbecher C. The Neuroplastin adhesion molecules: key regulators of neuronal plasticity and synaptic function. Journal of neurochemistry. 2014; 131:268–283. [PubMed: 25040546]

38. Herrera-Molina R, et al. Structure of excitatory synapses and GABAA receptor localization at inhibitory synapses are regulated by neuroplastin-65. The Journal of biological chemistry. 2014; 289:8973–8988. [PubMed: 24554721]

39. Cheung CC, et al. Identification of BERP (brain-expressed RING finger protein) as a p53 target gene that modulates seizure susceptibility through interacting with GABA(A) receptors. Proc Natl Acad Sci U S A. 2010; 107:11883–11888. [PubMed: 20543135]

40. Giesemann T, et al. Complex formation between the postsynaptic scaffolding protein gephyrin, profilin, and Mena: a possible link to the microfilament system. The Journal of neuroscience : the official journal of the Society for Neuroscience. 2003; 23:8330–8339. [PubMed: 12967995]

41. Murk K, et al. Neuronal profilin isoforms are addressed by different signalling pathways. PLoS One. 2012; 7:e34167. [PubMed: 22470532]

42. Pilgram GS, Potikanond S, Baines RA, Fradkin LG, Noordermeer JN. The roles of the dystrophin-associated glycoprotein complex at the synapse. Mol Neurobiol. 2010; 41:1–21. [PubMed: 19899002]

43. Akshoomoff N, Mattson SN, Grossfeld PD. Evidence for autism spectrum disorder in Jacobsen syndrome: identification of a candidate gene in distal 11q. Genet Med. 2015; 17:143–148. [PubMed: 25058499]

44. Epi KC, et al. De novo mutations in epileptic encephalopathies. Nature. 2013; 501:217–221. [PubMed: 23934111]

45. Weaving LS, et al. Mutations of CDKL5 cause a severe neurodevelopmental disorder with infantile spasms and mental retardation. Am J Hum Genet. 2004; 75:1079–1093. [PubMed: 15492925]

46. Fehr S, et al. The CDKL5 disorder is an independent clinical entity associated with early-onset encephalopathy. Eur J Hum Genet. 2013; 21:266–273. [PubMed: 22872100]

47. Falace A, et al. TBC1D24, an ARF6-interacting protein, is mutated in familial infantile myoclonic epilepsy. Am J Hum Genet. 2010; 87:365–370. [PubMed: 20727515]

48. Rehman AU, et al. Mutations in TBC1D24, a gene associated with epilepsy, also cause nonsyndromic deafness DFNB86. Am J Hum Genet. 2014; 94:144–152. [PubMed: 24387994]

49. Shirley MD, et al. Sturge-Weber syndrome and port-wine stains caused by somatic mutation in GNAQ. N Engl J Med. 2013; 368:1971–1979. [PubMed: 23656586]

50. Quemener-Redon S, et al. A small de novo 16q24.1 duplication in a woman with severe clinical features. Eur J Med Genet. 2013; 56:211–215. [PubMed: 23333879]

51. Basel-Vanagaite L, et al. The CC2D1A, a member of a new gene family with C2 domains, is involved in autosomal recessive non-syndromic mental retardation. J Med Genet. 2006; 43:203–210. [PubMed: 16033914]

52. Mory A, et al. A nonsense mutation in the human homolog of Drosophila rogdi causes Kohlschutter-Tonz syndrome. Am J Hum Genet. 2012; 90:708–714. [PubMed: 22482807]

53. Schossig A, et al. Mutations in ROGDI Cause Kohlschutter-Tonz Syndrome. Am J Hum Genet. 2012; 90:701–707. [PubMed: 22424600]

54. Feng G, et al. Dual requirement for gephyrin in glycine receptor clustering and molybdoenzyme activity. Science (New York, NY). 1998; 282:1321–1324.

55. Tomioka NH, et al. Elfn1 recruits presynaptic mGluR7 in trans and its loss results in seizures. Nat Commun. 2014; 5:4501. [PubMed: 25047565]

56. Nakatsu F, et al. Defective function of GABA-containing synaptic vesicles in mice lacking the AP-3B clathrin adaptor. The Journal of cell biology. 2004; 167:293–302. [PubMed: 15492041]

57. Uezu A, et al. Modified SH2 domain to phototrap and identify phosphotyrosine proteins from subcellular sites within cells. Proc Natl Acad Sci U S A. 2012; 109:E2929–2938. [PubMed: 23027962]

58. Kim IH, et al. Spine pruning drives antipsychotic-sensitive locomotion via circuit control of striatal dopamine. Nat Neurosci. 2015; 18:883–891. [PubMed: 25938885]

59. Kim IH, et al. Disruption of Arp2/3 results in asymmetric structural plasticity of dendritic spines and progressive synaptic and behavioral abnormalities. The Journal of neuroscience : the official journal of the Society for Neuroscience. 2013; 33:6081–6092. [PubMed: 23554489]

60. Westphal RS, Soderling SH, Alto NM, Langeberg LK, Scott JD. Scar/WAVE-1, a Wiskott-Aldrich syndrome protein, assembles an actin-associated multi-kinase scaffold. EMBO J. 2000; 19:4589–4600. [PubMed: 10970852]

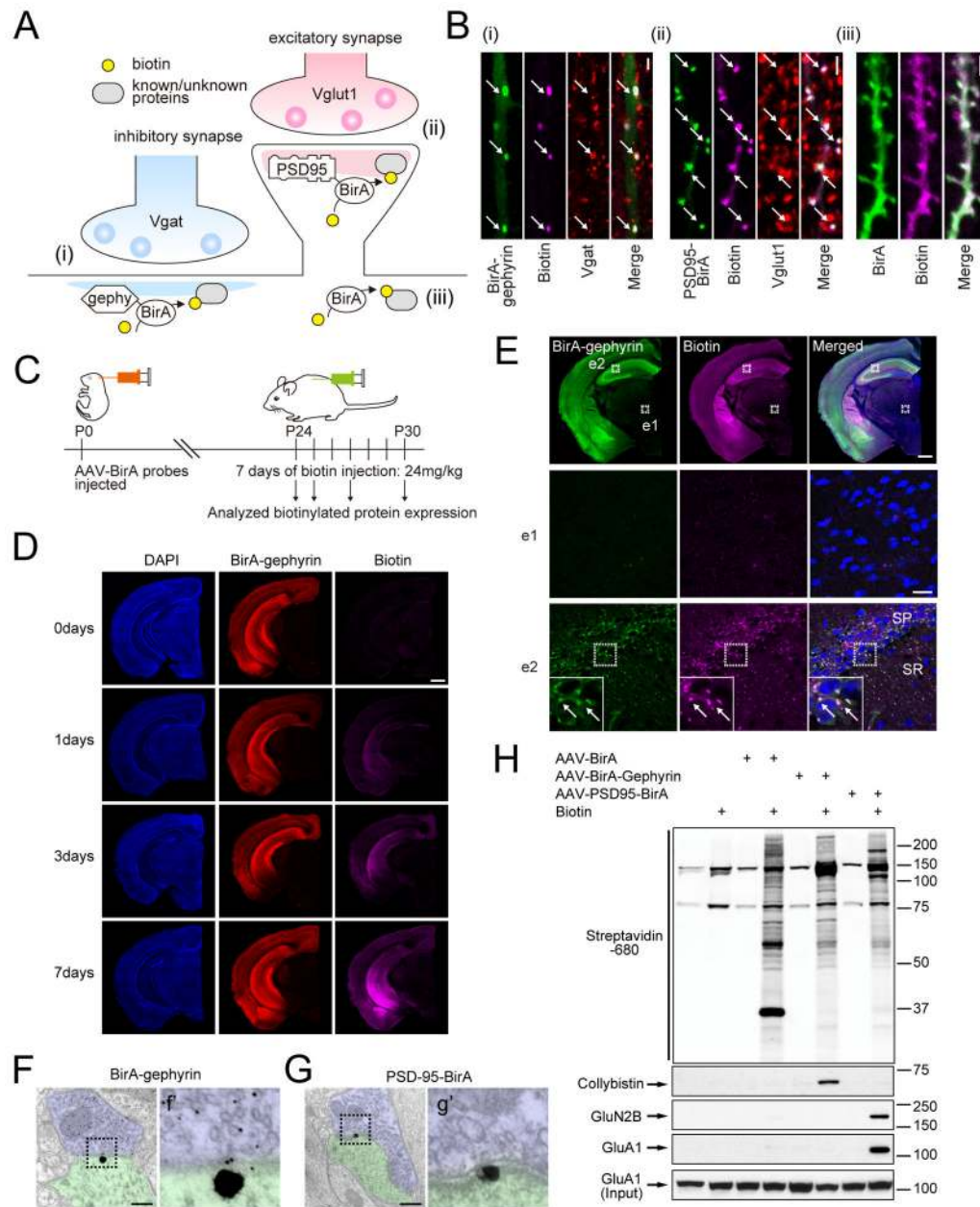61. Risher WC, et al. Astrocytes refine cortical connectivity at dendritic spines. Elife. 2014; 3

Fig. 1. Development of iBioID for synaptic proteomics

(**A**) Schematic of the iBioID approach for synapses. (**B**) Validation of BirA constructs in hippocampal slice using (i) BirA-gephyrin and (ii) PSD-95-BirA (white arrows point to colocalized puncta). (iii) BirA alone non-specifically labels proteins. Scale bar, 2 μm. (**C**) Outline of iBioID method in mice. (**D**) Successful biotinylation of proteins *in vivo* following i.p. biotin administration. Scale bar, 0.5 mm (**E**) Biotinylation is specific to regions expressing BirA-gephyrin (coronal section). Insets from thalamus (e1) and hippocampus (e2) and insets of e2 are shown. Scale bar top panel, 0.5 mm; e1 and e2, 20 μm. Electron micrographs verify enrichment of biotinylation at (**F, f′**) inhibitory or (**G, g′**) excitatory PSD substructures. Large gold beads, streptavidin labeling; small gold beads, immunolabel for

GABA. Scale bar, 250 nm. (**H**) Specific purification of known PSD proteins for each BirA fusion protein.
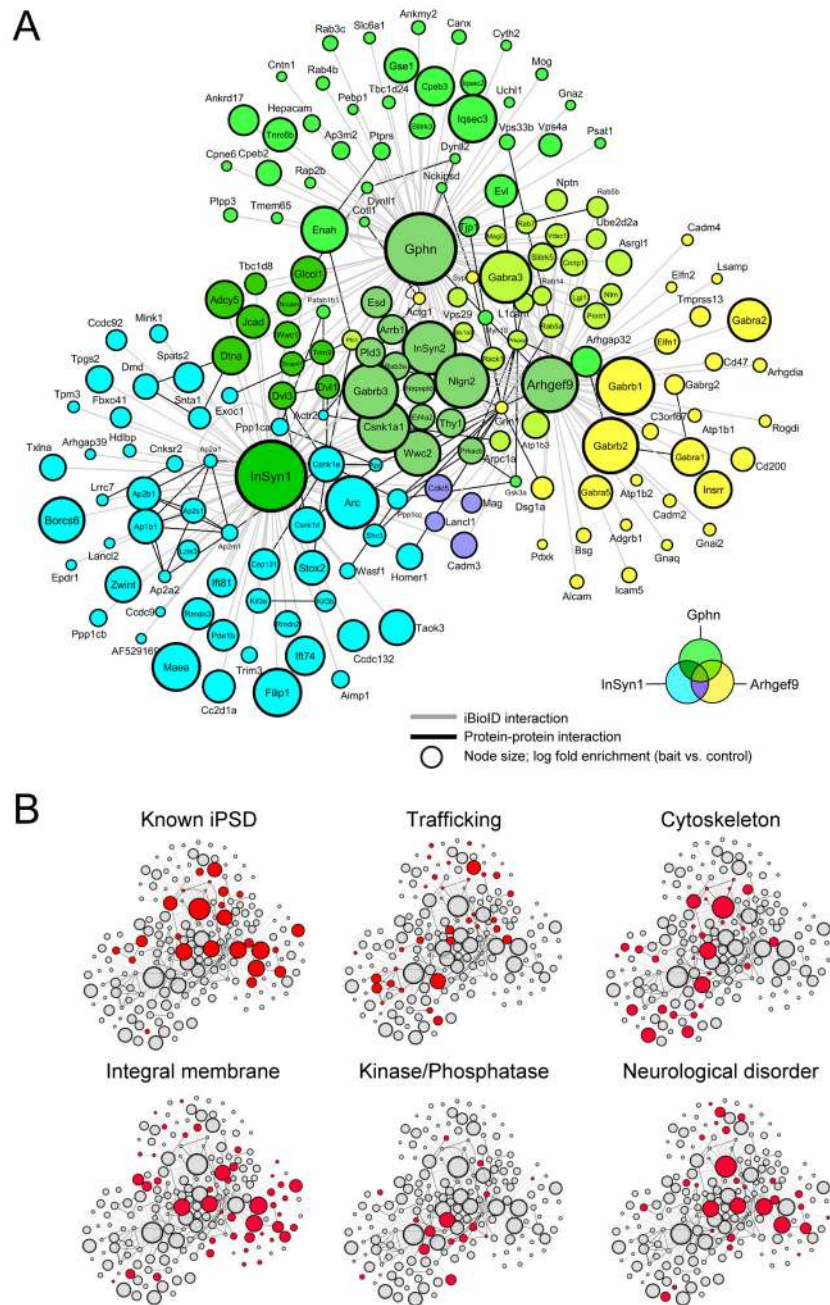
Fig. 2. Scale-free graph of the iPSD proteome

(**A**) InSyn1 (blue), gephyrin (green), and arhgef9 (yellow) BirA-dependent iBioID identifies a rich network of known and previously unknown proteins enriched at the iPSD. Node titles correspond to gene name; size represents fold-enrichment over negative control. Edges are shaded according to the types of interactions (grey, iBioID; black, protein-protein interactions previously reported). (**B**) Clustergram topology of iPSD proteins (red) in selected functional categories.
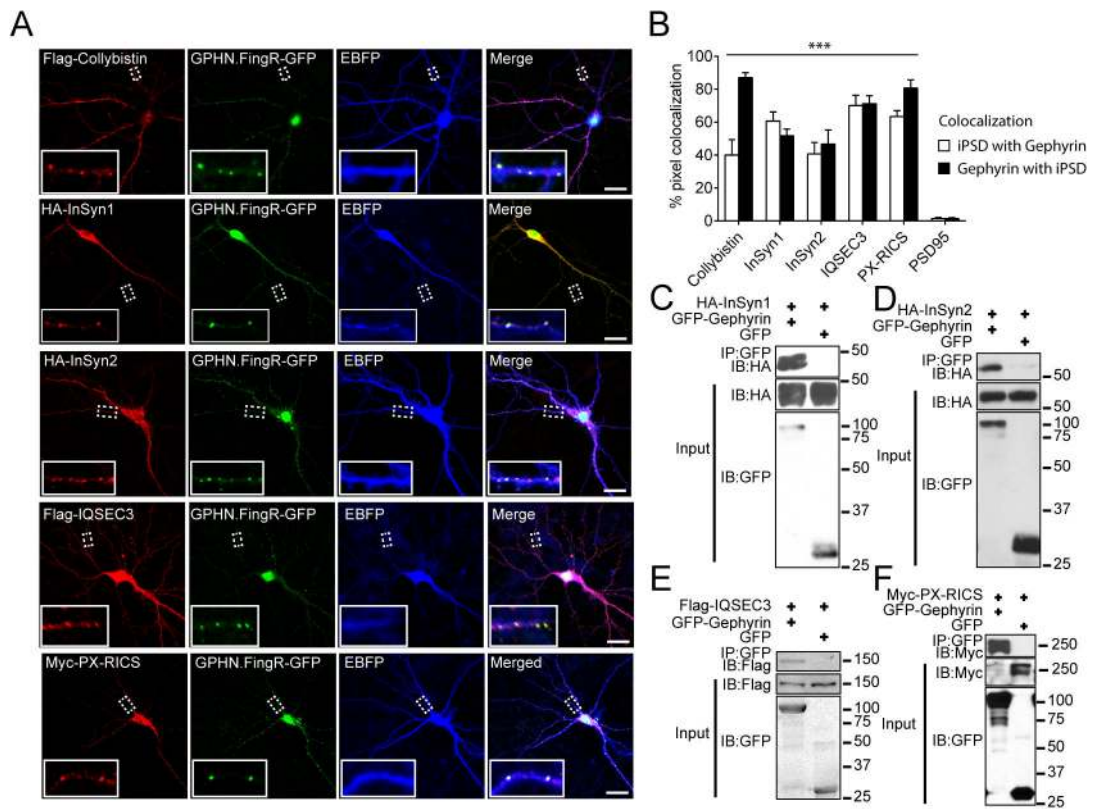
Fig. 3. Validation of selected iPSD proteins

(**A**) Co-localization of iPSD proteins (left column) with endogenous gephyrin (right column) in hippocampal neurons. Scale bar, 10 μm. (**B**) Each iPSD protein significantly co-localizes with gephyrin in dendrites compared to PSD95 (*n* > 9 dendritic ROIs). (**C–F**) iPSD proteins co-immunoprecipitate with gephyrin when co-expressed in HEK293 cells. ***p<0.001 one-way ANOVA followed by Dunnett's multiple comparisons test (B). Error bars ± SEM.
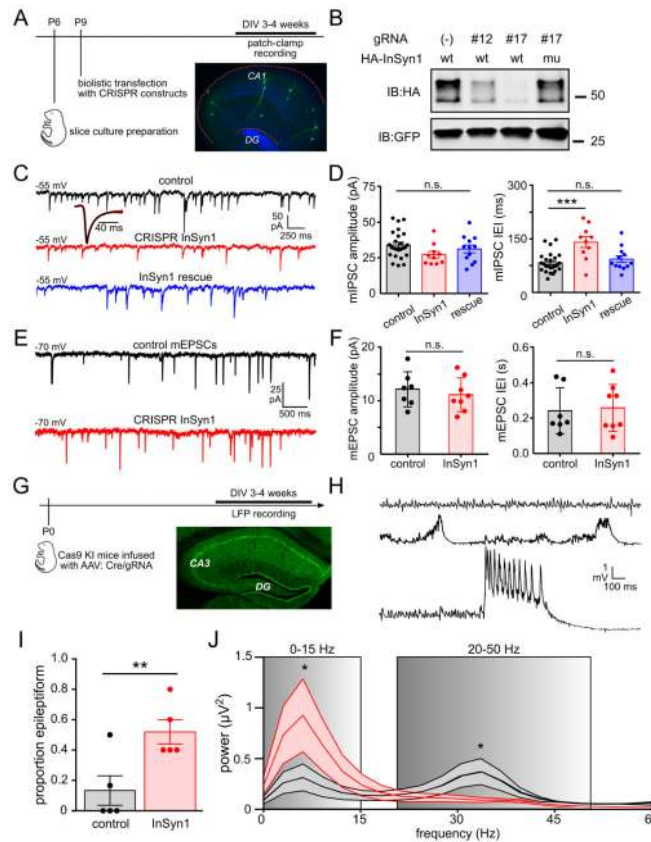
Fig. 4. Abnormal synaptic inhibition follows loss of the iPSD protein InSyn1

(**A**) Experimental schematic for panels C–F. (**B**) Validation of InSyn1 gRNAs (#12 & #17) and rescue constructs by 293T co-transfection and immunoblotting. (**C, D**) GABA$_A$-dependent miniature inhibitory postsynaptic currents (GABA$_A$ mIPSCs) recorded from CA1 pyramidal cells. Inset shows GABA$_A$ mIPSC waveform averages. InSyn1 depletion did not alter mIPSC kinetics (rise: control = 3.6 ± 0.6 ms, InSyn1 = 3.4 ± 0.6 ms, p = 0.51; decay: control = 9.7 ± 2.1 ms, InSyn1 = 10.3 ± 1.8 ms, p = 0.42). IEIs of InSyn1-depleted GABA$_A$ mIPSCs (*red*) are specifically increased compared to control (*black*) and rescue (*blue*) neurons. (**E, F**) AMPAR-dependent miniature EPSCs are not altered in InSyn1 depleted neurons. (**G**) Time-line schematic for local field potential (LFP) recordings in acute slices from Cas9 knock-in (KI) mice infected with AAV:Cre/Insyn1 gRNA. Image shows representative extent of AAV infection in hippocampus. (**H**) Representative LFP activities recorded in hippocampal area CA3 in the presence of 10 μM carbachol to model "awake state" gamma rhythm. *Top trace:* pure 30–40 Hz gamma oscillation; *middle trace*: 3–5 Hz spike-wave discharges; *bottom trace*: ictal-like burst – the latter two indicative of hyperexcitable or epileptiform activity. (**I**) InSyn1 gRNA expressing slices exhibit increased epileptiform activity. (**J**) Averaged power spectra showing signal energy in the InSyn1 gRNA expressing slices is increased in the 0–15 Hz frequency band and decreased in the 20–50 Hz frequency bands. *p<0.05, **p<0.01, ***p<0.001, n.s. = not statistically significant. Error bars ±SEM.
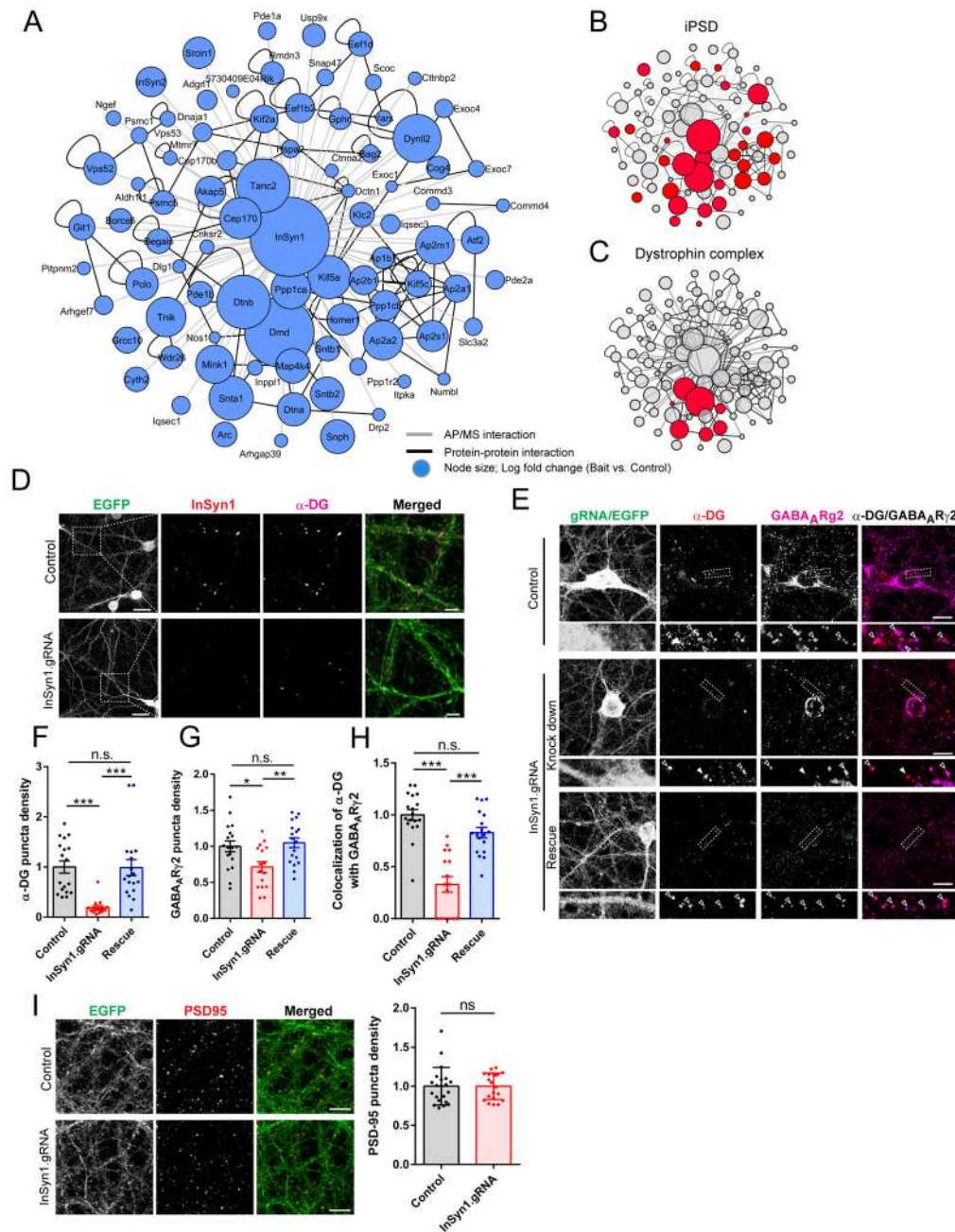
Fig. 5. InSyn1 functionally associates with the dystrophin complex at the iPSD

(**A**) Network analysis of affinity purified InSyn1-GFP proteome from mouse brain. (**B**, **C**) Clustergram topologies of InSyn1 associated proteins in selected functional categories. (**D**) Co-localization of InSyn1 with α-dystroglycan (α-DG) is diminished after depleting InSyn1 with Cas9 conditional knock-in hippocampal neurons infected with AAV:Cre/Insyn1 gRNA. Scale bar, 10 μm. (**E**) InSyn1 is essential for GABA$_A$R and α-DG cluster density. Cas9 KI hippocampal neurons were stained for GABA$_A$Rγ2 and α-DG following infection with control AAV:Cre/(-)gRNA (top panel, Control); AAV:Cre/Insyn1 gRNA (middle panel, Knockdown), or AAV:Cre/Insyn1 gRNA, and transfected with InSyn1 gRNA resistant

plasmid (bottom panels, Rescue). Insets show higher magnification regions with open (colocalized puncta) and closed (non-colocalized puncta) arrows. (**F, H**) Quantification of α-DG and $GABA_AR\gamma2$ puncta co-localization or density (n=16–18). *p<0.05, **p<0.01, ***p<0.001 one-way ANOVA followed by Tukey's multiple comparisons test (F–H). Error bars ± SEM. Scale bar, 10 μm. (**I**) Loss of InSyn1 does not alter PSD-95 puncta density. Cas9 knock-in hippocampal neurons infected with AAV:Cre/Insyn1 gRNA were stained with PSD-95 and quantified (n = 18–20 neurons). n.s = not significant, two-tailed *t*-test (I).